AD-A232 193

REPORT DOCUMENTATION PAGE

Form Approved
OMB No. 0704-0188

1. Agency Use Only *(Leave blank).*	2. Report Date. 1990	3. Report Type and Dates Covered. Proceedings

	5. Funding Numbers.
Title and Subtitle. athymetric analysis of "in-water" upwelling radiance data	*Program Element No* 62435N *Project No.* RM25G85
Author(s). Temple H. Fay and H. Vincent Miller	*Task No* 801 *Accession No* DN255031

7. Performing Organization Name(s) and Address(es). Naval Oceanographic and Atmospheric Research Laboratory Ocean Sciences Directorate Stennis Space Center, MS 39529-5004	8. Performing Organization Report Number. PR 89:060:351

9. Sponsoring/Monitoring Agency Name(s) and Address(es). Naval Oceanographic and Atmospheric Research Laboratory Ocean Sciences Directorate Stennis Space Center, MS 39425-5004	10. Sponsoring/Monitoring Agency Report Number. PR 89:060:351

DTIC
ELECTE
MAR 1 6
S
G
Distribution Code.

11. Supplementary Notes.
SPIE

12a. Distribution/Availability Statement.
Approved for public release; distribution is unlimited.

13. Abstract *(Maximum 200 words).*

In June 1988, the Naval Ocean Research and Development Activity (NORDA) collected some "in-water" data using its Towed Underwater Pumping System (TUPS) in the near-shore waters off St. Andrews State Park, Shell Island, Florida. These in situ data include latitude; longitude; depth in meters; narrow-band upwelling at 465 nm, 507 nm, and 532 nm; broad-band downwelling collected at the surface; temperature; salinity; and transmissivity. In this paper, we investigate the relationship between depth and the normalized upwelling irradiance (upwelling divided by downwelling) in the three bands. Algorithms used to calculate water depth from remotely sensed airborne and satellite multispectral data are applied to the TUPS data and results compared. The TUPS data have the advantage over most aircraft-- and satellite -- collected data because they were collected over an essentially uniform bottom type (smooth sandy bottom with steady slope) and have no atmospheric contamination. A new algorithm for depth calculation is proposed.

14. Subject Terms. (U) Algorithms; (U) Multispectral; (U) Atmospheric Contamination	15. Number of Pages. 14
	16. Price Code.

17. Security Classification of Report. Unclassified	18. Security Classification of This Page. Unclassified	19. Security Classification of Abstract. Unclassified	20. Limitation of Abstract. SAR

91 2 11 180

DTIC FILE COPY

Reprinted from

Ocean Optics X

16–18 April 1990
Orlando, Florida

P

Volume 1302

Bathymetric analysis of "in—water" upwelling radiance data

Temple H. Fay and H. Vincent Miller

Naval Oceanographic and Atmospheric Research Laboratory
Stennis Space Center, MS

R. Kent Clark

University of South Alabama, Mobile, AL

ABSTRACT

In June 1988, the Naval Ocean Research and Development Activity (NORDA) collected some "in—water" data using its Towed Underwater Pumping System (TUPS) in the near—shore waters off St. Andrews State Park, Shell Island, Florida. These *in situ* data include latitude; longitude; depth in meters; narrow—band upwelling at 465 nm, 507 nm, and 532 nm; broad—band downwelling collected at the surface; temperature; salinity; and transmissivity. In this paper, we investigate the relationship between depth and the normalized upwelling irradiance (upwelling divided by downwelling) in the three bands. Algorithms used to calculate water depth from remotely sensed airborne and satellite multispectral data are applied to the TUPS data and results compared. The TUPS data have the advantage over most aircraft— and satellite—collected data because they were collected over an essentially uniform bottom type (smooth sandy bottom with steady slope) and have no atmospheric contamination. A new algorithm for depth calculation is proposed.

1. INTRODUCTION

Over the past few years, the Naval Oceanographic and Atmospheric Research Laboratory (NOARL), formerly the Naval Ocean Research and Development Activity (NORDA), has been developing and testing an Airborne Bathymetric Survey System (ABS) designed to measure water depth in coastal waters (see Hickman et al.[5]). The ABS integrates active laser soundings with simultaneously obtained, passive, multispectral scanner digital imagery. Algorithms extrapolate laser soundings and scanner data to scene—wide bathymetry. If sufficient accuracies can be obtained, then this technique would provide for inexpensive and rapid production of bathymetric charts for shallow—water areas.

To support the ABS project, to provide environmental data for ground truth, and to help improve ABS algorithms, NORDA conducted a field experiment in the near—shore waters off St. Andrews State Park near Panama City, Florida, in June 1988 (see Guinasso and Wiesenburg[4]). In this field experiment, NORDA's Towed Underwater Pumping System (TUPS) was used to collect a variety of environmental data, including water depth and upwelling irradiance, in three narrow spectral bands centered at 465 nm, 507 nm, and 532 nm. Data were collected on the south side of Shell Island (St. Andrews State Park) on 19 and 20 June 1988.

In this paper we investigate current multispectral algorithms employed for shallow—water bathymetry using the TUPS data; in particular, we investigate the relationship between depth and the normalized upwelling irradiance (upwelling divided by downwelling) in the three bands. The bathymetry models discussed here are based on the fact that sunlight is exponentially attenuated twice as it passes through the water column and is reflected off the bottom. Given a data base of known depths at known positions, and given multispectral imagery that encompasses the data base, one regresses the model against the image values and the depth data base to

determine model parameters, which then can be applied to all positions in the imagery. The TUPS data have the advantage over most data collected by aircraft or satellite in that they were collected over relatively clear water with an essentially uniform bottom type (smooth sandy bottom with steady slope from the beach to deeper water $\approx$ 25 m) and have no atmospheric contamination. Some new algorithms for depth calculation are proposed as well. We also introduce a new technique, which incorporates an effective attenuation coefficient term which varies as a function of depth.

2. THE TOWED UNDERWATER PUMPING SYSTEM

The TUPS contains a depth sensor (0 − 100 m with 2−cm resolution) and narrow band (±10 nm) upwelling irradiance sensors at wavelengths 465 nm, 507 nm, and 532 nm. NORDA's TUPS Environmental Sensor System (TESS) was used to collect incident light measurements for normalization with the TUPS data. Employing two pyroheliometers, broadband downwelling irradiance data were collected simultaneously with the TUPS upwelling data. This downwelling measurement is important, since clouds overhead reduce the amount of light hitting the ocean surface and correspondingly reduce the amount of upwelling irradiance. Table 1 shows the sensor configuration of TUPS, and Table 2 shows the TESS configuration; these tables are adapted from Guinasso and Wiesenburg[4].

Throughout this paper, we will study various models relating normalized upwelling to water depth. The light signals shall be normalized irradiances in the sense that we take $L_\lambda = \mathscr{L}_\lambda / \rho 1$, where $\mathscr{L}_\lambda$ is the upwelling radiance (in $\mu W/cm^2/nm$) received on the TUPS and $\rho 1$ is the broadband downwelling radiance measured (in $\mu W/cm^2/nm$) at the surface by pyroheliometer 1 in the TESS. This normalized radiance is used to reduce such effects as clouds passing overhead. The notation L1, L2, L3 is used to denote these normalized upwelling irradiances in wavelengths 465 nm, 507 nm, 532 nm, respectively. Figure 1 shows the normalized upwelling versus depth. Table 3 shows part of the correlation matrix of TUPS and TESS measurements; for the full matrix see Guinasso and Wiesenburg[4]. The reader should note that the two pyroheliometers are over 99% correlated; hence, the choice of which to use for the normalization is immaterial. Also note that the three nonnormalized upwelling bands are over 97% correllated with each other. Thus, not much improvement of multiband algorithms over single band algorithms can be expected.

3. THE OPTICAL BATHYMETRY MODEL

In this discussion, we assume the simple radiance transfer model based on the Lambert−Beers Law, called herein the *Single Band Model* (also called Bouguer's Law[9] and Jerlov's Model[7]), in which the radiance in wavelength λ at water depth z is given by the equation

$$L_\lambda = L_{\lambda_\infty} + R_\lambda \exp(-f \cdot \kappa_\lambda \cdot z), \qquad (1)$$

where

$\quad L_\lambda$ is the received upwelling radiance value in the wavelength λ,

$\quad L_{\lambda_\infty}$ is the observed radiance over optically deep water,

$\quad R_\lambda$ is a radiance term that is sensitive to bottom reflectance,

$\quad \kappa_\lambda$ is an effective water attenuation coefficient at wavelength λ,

f is a geometrical constant relating the angle of solar incidence and the sensor viewing angle and $f = 2$ for nadir view with sun at zenith.

Solving for z in equation (1) yields

$$z = (\log(R_\lambda) - \log(L_\lambda - L_{\lambda\infty}))/(f \cdot \kappa_\lambda) \tag{2}$$

where $\log(-)$ stands for the natural logarithm. The difficulty in calculating water depth directly from equation (2) is that the values of R_λ and κ_λ are generally not known. With the notation $X_\lambda = \log(L_\lambda - L_{\lambda\infty})$, the depth equation is recast in the regression form

$$z = A + B \cdot X_\lambda, \tag{3}$$

where A and B are coefficients to be determined by regressing the equation against known ground truth, minimizing the difference between the known depths and the depths calculated from equation (3) using measured light signals L_λ and $L_{\lambda\infty}$. In order to do this regression, it is assumed that both R_λ and κ_λ are constant over the ground truth.

Paredes and Spero[8] generalized this technique into a multiband algorithm to improve performance by reducing the sensitivity of the algorithm due to variation in bottom reflection. They suggested that it is possible to include information contributed from multiple spectral bands by forming a weighted sum of single–band depth solutions as given by equation (3). We write for n wavelengths,

$$z = \sum_1^n \omega_i \cdot [(1/f \cdot \kappa_i) \cdot (\log(R_i) - X_i)], \text{ with } \sum_1^n \omega_i = 1. \tag{4}$$

This immediately generalizes to a (regression) model in the form

$$z = A_0 + \sum_1^n A_i \cdot X_i, \tag{5}$$

where the constants A_i are determined to minimize the error between the model–predicted depths and the measured depths at the ground truth control points. Clark et al.[2] demonstrated this model's improved performance using Landsat Thematic Mapper imagery, and experiments reported in Clark et al.[3] add further evidence to this improvement.

Using the TUPS normalized upwelling bands L1, L2, and L3, we performed single–band regression fits of equation (3) and two– and three–band regression fits of equation (4) with $n = 2$ and 3. The results are tabulated in Tables 4, 5, and 6. In these tables, the term RM stands for the statistical (multiple) correlation coefficient and the term RMS is the root mean square of the error (calculated depth minus calibration depth).

The following Figure 2 shows scatter plots of both $\log(L1)$ and $\log(L1 - L1_{min})$. Note that the scatter plot of $\log(L1)$ has roughly constant slope for $3 \leq z \leq 10$ m, and that in the scatter plot of $\log(L1 - L1_{min})$, the spread of the plot increases dramatically after 10 m. This

suggests that $\kappa 1$ is not constant and that the errors in computing the bathymetry will increase as we take the computations deeper. Similar effects are seen in scatter plots for bands $L2$ and $L3$.

4. AN EMPIRICAL MODEL

From the single—band model, a graph of the radiance in the wavelength λ versus water depth z can be expected to have the appearance illustrated in Figure 3. Here, we assume z_{max} is sufficiently deep so that the signal received at this depth is solely due to scattering within the water column (no bottom reflectance). Thus, based on the Lambert—Beers Law, we expect to see a curve of the form

$$L_\lambda = A \cdot \exp(-2 \cdot \kappa_\lambda \cdot z) + B, \tag{6}$$

where

$$\underset{z \to z_{max}}{Lim} L_\lambda = \underset{z \to \infty}{Lim} L_\lambda = L_{min} = B \quad and \tag{7}$$

$$\underset{z \to z_{min}}{Lim} L_\lambda = L_{max} = A \cdot \exp(-2 \cdot \kappa_\lambda \cdot z_{min}) + L_{min}, \tag{8}$$

from which it follows that

$$L_\lambda = L_{min} + (L_{max} - L_{min}) \cdot \exp(-2 \cdot \kappa_\lambda \cdot (z - z_{min})), \tag{9}$$

which agrees with the model given in equation (1) by setting $L_{min} = L_{\lambda\infty}$ and $R_\lambda = (L_{max} - L_{min}) \cdot \exp(2 \cdot \kappa_\lambda \cdot z_{min})$. Letting $\Delta L = L_{max} - L_{min}$ and dropping the subscript λ, we have the equation

$$L = L_{min} + \Delta L \cdot \exp(-2 \cdot \kappa \cdot (z - z_{min})), \tag{10}$$

which we shall call the *empirical equation*. From this equation it is easy to solve for κ obtaining,

$$\kappa = 0.5 \cdot [\log(\Delta L) - \log(L - L_{min})]/(z - z_{min}). \tag{11}$$

From an examination of the values of L1, we empirically obtained

$$L1_{max} = 4.827 \quad when \quad z_{min} = 1.5 \ m, \ L1_{min} = 0.320. \tag{12}$$

Substituting the values for L1 into equation (11) and plotting κ versus depth by plugging in the TUPS data values, we obtained Figure 4. It is important to observe that here $\kappa 1$ represents an overall effective attenuation coefficient and not the *diffuse attenuation coefficient*. Moreover, these empirical $\kappa 1$ values are calculated from different spatial locations that have various associated depths as opposed to most diffuse attenuation calculations, which are made at a single spatial location and where an instrument is lowered to different depths to calculate an attenuation profile.

From a visual inspection of this scatter plot for $\kappa 1$, it appears that the data tend toward a horizontal asymptote as z increases and may approach a vertical asymptote as the depth nears zero, although having no data for depths less than 1.3 m makes this assumption subjective. Furthermore, the noise and spread in the signals of L1, L2, and L3 for depths less than 3 m concomitantly causes noise and signal spread in the scatter plots of $\kappa 1$, $\kappa 2$, and $\kappa 3$. However, these observations and the fact that κ is measured in inverse meters suggest fitting a hyperbolic curve of the form

$$\kappa = A/z + B \tag{13}$$

through the data. Moreover, substituting equation (13) into equation (6) yields

$$L = L_{min} + \exp(-2 \cdot (A/z + B) \cdot (z - z_{min})) \tag{14}$$

from which it is possible to solve for z in terms of L. In doing so, one obtains the quadratic equation

$$B \cdot z^2 + (A - B \cdot z_{min} - \log(Y)) \cdot z - A \cdot z_{min} = 0, \tag{15}$$

where we have let $Y = (\Delta L/(L - L_{min}))^{1/2}$ for notational simplicity. Using the quadratic formula, we obtain

$$z = \{1/2 \cdot B\} \cdot \{\log(Y) + B \cdot z_{min} - A \pm [\log(Y) \cdot (\log(Y) + 2 \cdot B \cdot z_{min} - 2 \cdot A)$$
$$+ (B \cdot z_{min} + A)^2]^{1/2}\}. \tag{16}$$

There are, of course, two solutions to the quadratic equation expressed in (15). It turns out that in taking the solution corresponding to the minus sign, we obtain negative values for z so that this solution is extraneous, and we need only consider the solution with the plus sign.

There are several ways to estimate the unknowns A and B. One way would be to select, presumably judiciously, two points (z_1, κ_1) and (z_2, κ_2) and determine A and B from simultaneously solving two equations. Alternatively, one can estimate B by looking at the data for depths greater than 20 m, and then just one additional point (z_1, κ_1) with z_1 small is sufficient to calculate A. Another way would be to perform a least–squares fit of the functional form $\kappa = A/z + B$ to the data.

Yet still another way to approach the determination of A and B, which produced good results, is to minimize the square error produced from equation (15). That is, given a data point (z_i, L_i) from one of the bands, substitution of (z_i, L_i) into the quadratic equation (11) will yield, not 0, but some presumably small error ϵ_i. Summing the squares of these errors we have

$$\sum [B \cdot z_i^2 + (A - B \cdot z_{min} - \log(Y_i)) \cdot z_i - A \cdot z_{min}]^2 = \sum \epsilon_i^2, \tag{17}$$

where again, $Y_i = (\Delta L/(L_i - L_{min}))^{1/2}$ for notational convenience. By taking partial derivatives with repect to A and B and setting them equal to 0, we obtain the equations

$$A \cdot \sum (z_i - z_{min})^2 + B \cdot \sum z_i \cdot (z_i - z_{min})^2 = \sum \log(Y_i) \cdot z_i \cdot (z_i - z_{min}), \tag{18}$$

$$A \cdot \sum z_i \cdot (z_i - z_{min})^2 + B \cdot \sum z_i^2 \cdot (z_i - z_{min})^2 = \sum \log(Y_i) \cdot z_i^2 \cdot (z_i - z_{min}), \tag{19}$$

which are easy to solve for A and B. Applying this technique, we restrict the input data points (z_i, L_i) to have, for example, $3 \leq z_i \leq 10$, thus avoiding the noisy data for $z_i < 3$ and, for $z_i > 10$, the problem of small variations in the signal L_i, producing large variations in the depth z_i. The upper bound may be changed according to which band is used; we used 10 for L1 and 17 for L2 and L3. These values were chosen because the scatter plots of L1, L2, and L3 flatten out at approximately these depths; thus, the greatest variation in the signal versus depth occurs for values less than these thresholds.

In Table 7, results of employing this technique are given. Figure 5 shows the curve generated by this technique plotted over the data for bands L1. Figure 6 shows the error plotted versus depth. Note that for water depths less than 3 m, the error is large, as is the error for depths greater than 10 m. The reason for this is the noise in the signal in the shallowest depths, and for the deeper water, very small changes in the signal value correspond to large changes in the depth value. In Figure 7 this phenomenon can be seen as well. Similar results are obtained for bands L2 and L3, with the error becoming larger at approximately 17 m.

5. CONCLUSIONS

The TUPS data, collected *in situ*, display the expected form predicted by the Lambert—Beers Law. Some minor variations are accounted for by either being in shallow water (less than 3 m) where the signals are noisy, or in deeper water (roughly speaking, greater than 10m) which appears to have a different effective attenuation coefficient than that for water depths in the 3— to 10—m range (the deeper water is clearer).

In an attempt to allow for changes in the effective attenuation coefficient κ, we have introduced a new regression model based on κ having a hyperbolic form. This technique differs from the classical single—band bathymetric regression technique, in that one chooses an L_{max} at a z_{min} value, a somewhat subjective choice. Both techniques require one to choose a value for L_{min}. The results reported here show that both methods perform equally well on the TUPS data, with the new technique slightly better overall. This improvement is due to a slightly better fit in the shallow water (less than 3 m) and because the bathymetry curve is forced to pass through the point (z_{min}, L_{max}). A multiband approach can likely be developed using this new regression technique. This development may improve the bathymetric information extraction for such noisier data as LANDSAT Thematic Mapper imagery.

6. ACKNOWLEDGEMENT

TUPS data. NOARL Contribution Number PR 89:060:351. (This document has been approved for public release.)

7. REFERENCES

1.   J. M. Chambers, W. S. Cleveland, B. Kleiner, and P. A. Tukey, *Graphical Methods for Data Analysis*, Duxbury Press, Boston, 1983.

2.   R. K. Clark, T. H. Fay, and C. L. Walker, "Shallow water bathymetry models using multispectral digital data," *Journal of Imaging Technology*, to appear 1990.

3.   R. K. Clark, T. H. Fay, and C. L. Walker, "Bathymetry Calculations from Landsat TM Imagery Under a Generalized Ratio Assumption," *Applied Optics*, vol. 26, p.4036, 1987.

4.   N. L. Guinasso, Jr. and D. A. Wiesenburg, "Analysis of nearshore bathymetry and optical data from TUPS," *Texas A & M Univ. GERG Technical Report* L 88–174, 1988.

5.   G. D. Hickman, M. M. Harris, D. Durham, and R. K. Clark, "The Airborne Bathymeric Survey System," *Marine Technology Society Journal*, vol.20, #2, 1986, 5–13.

6.   N. G. Jerlov, *Optical Oceanography*, Elsevier, New York, 1976.

7.   D. R. Lyzenga, "Passive remote sensing techniques for mapping water depth and bottom features," *Applied Optics*, vol. 17, p. 379, 1978.

8.   J. M. Paredes and R. E. Spero, "Water depth mapping from passive remote sensing data under a generalized ratio assumption," *Applied Optics*, vol. 22, p.1134, 1983.

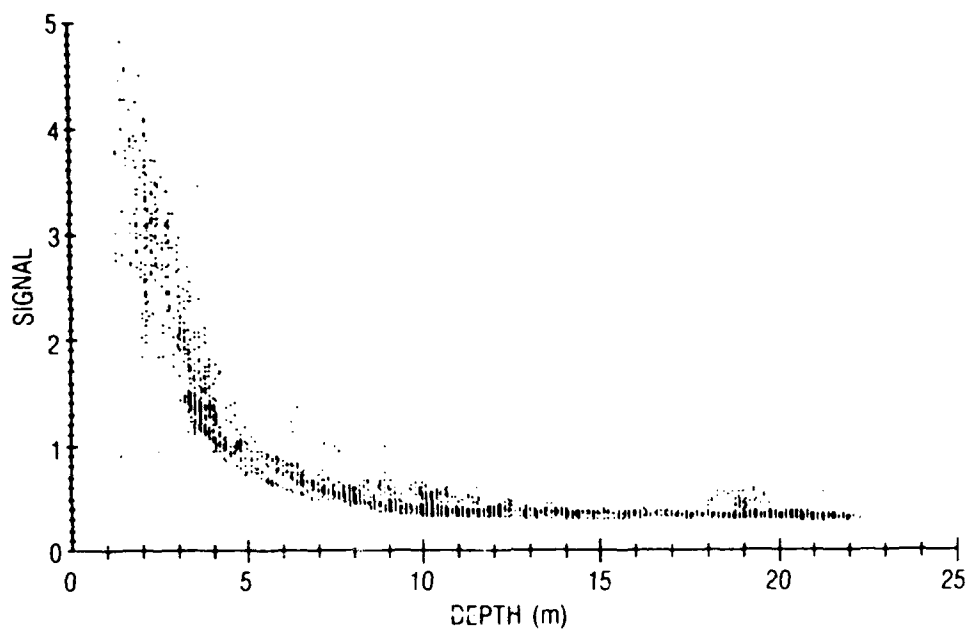9.   K. S. Shifrin, *Physical Optics of Ocean Waters*, Amer. Inst. Physics, NY, 1988.

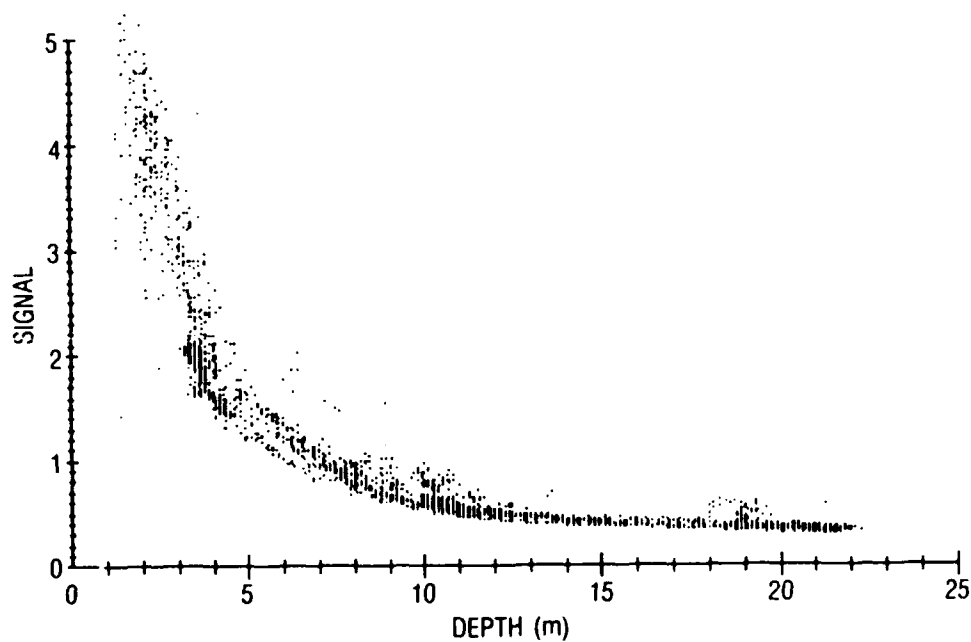Figure 1.1. Normalized upwelling L1 vs depth.

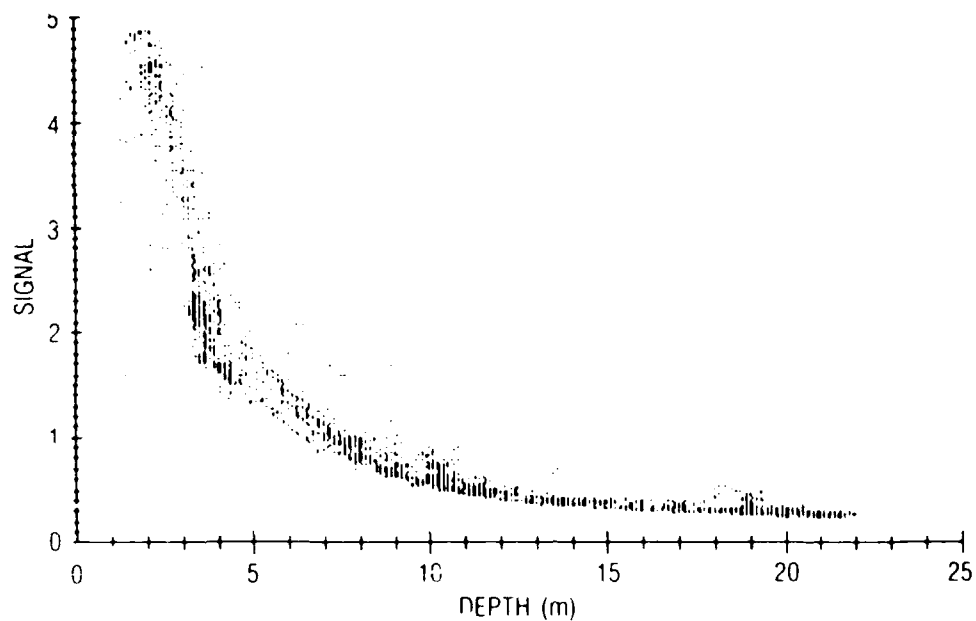Figure 1.2. Normalized upwelling L2 vs depth.
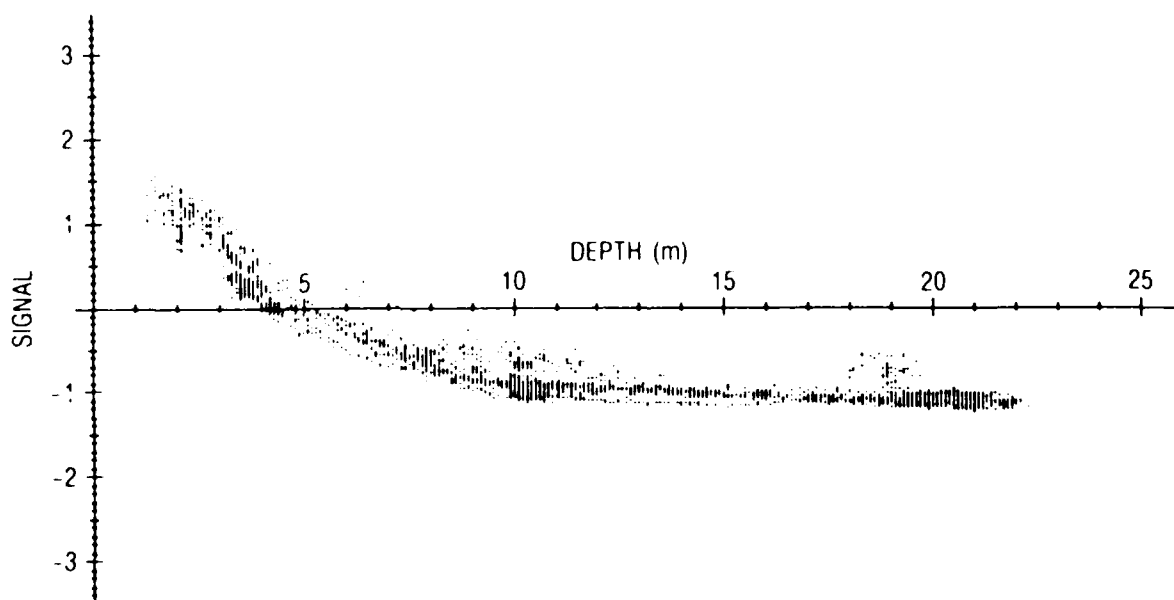
Figure 1.3. Normalized upwelling L3 vs depth.

Figure 2.1. Log (L1) vs depth.

Figure 2.2. Log (L1-0.320) vs depth.
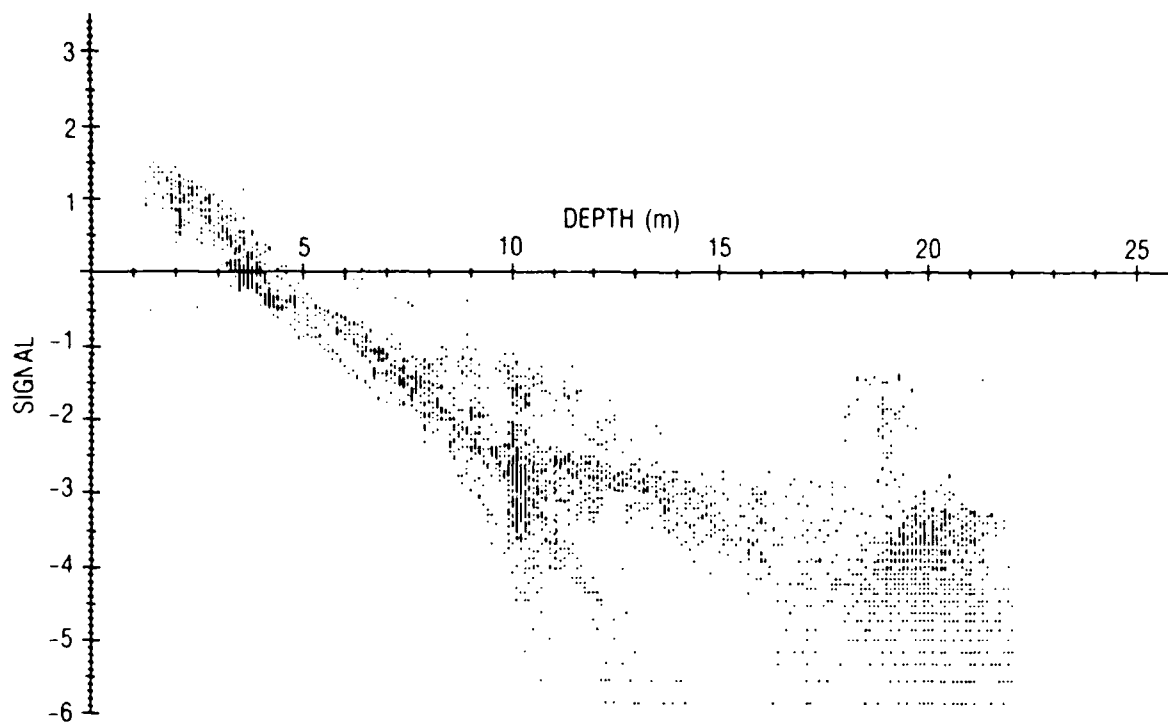

L vs DEPTH

EXPONENTIAL CURVE: $L = A \cdot exp(-2 \cdot k \cdot (z-z_{min})) + L_{min}$

$A = L_{max} - L_{min}$
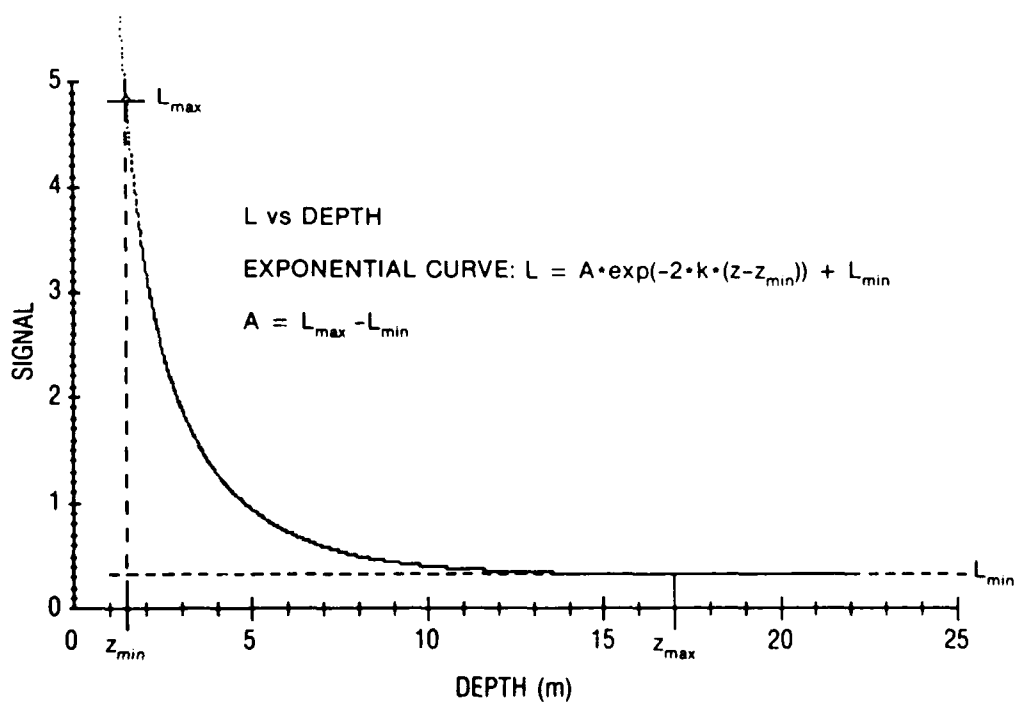
Figure 3. Empirical radiance curve.

Figure 4. k1 vs depth.

HYPERBOLIC k FIT, RMS = 0.751
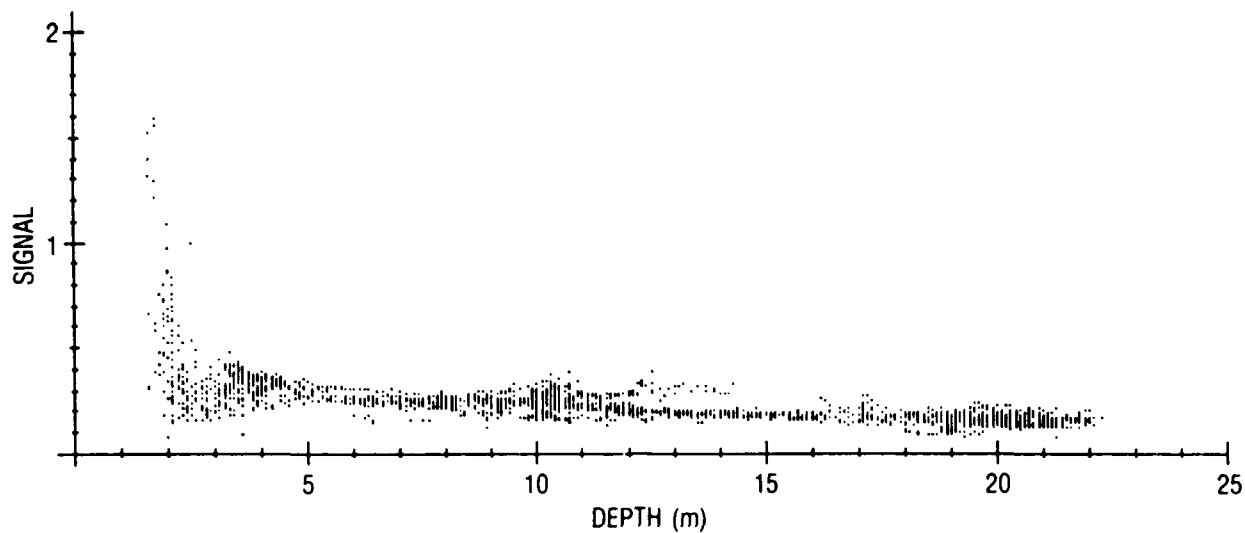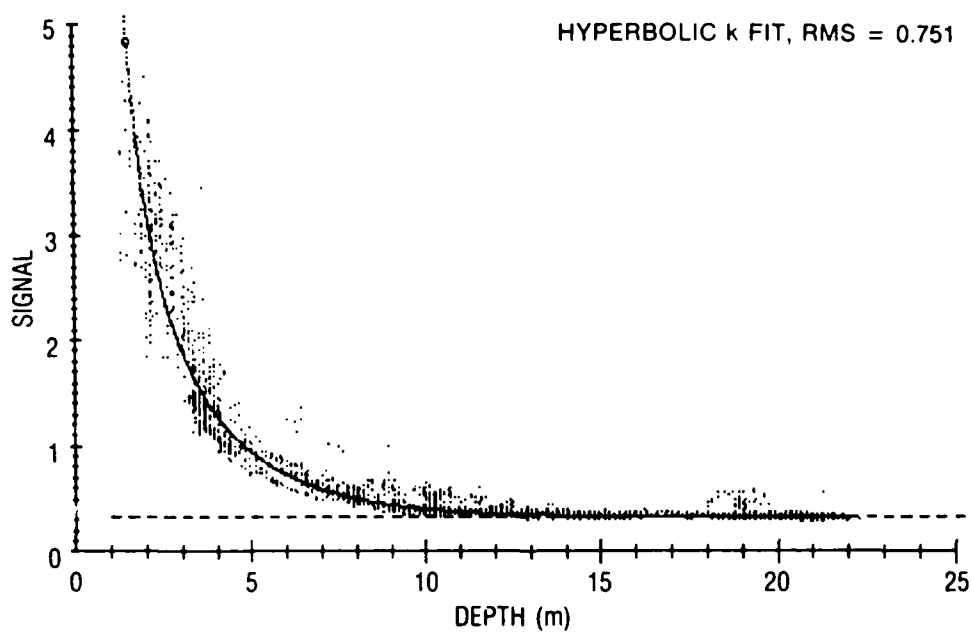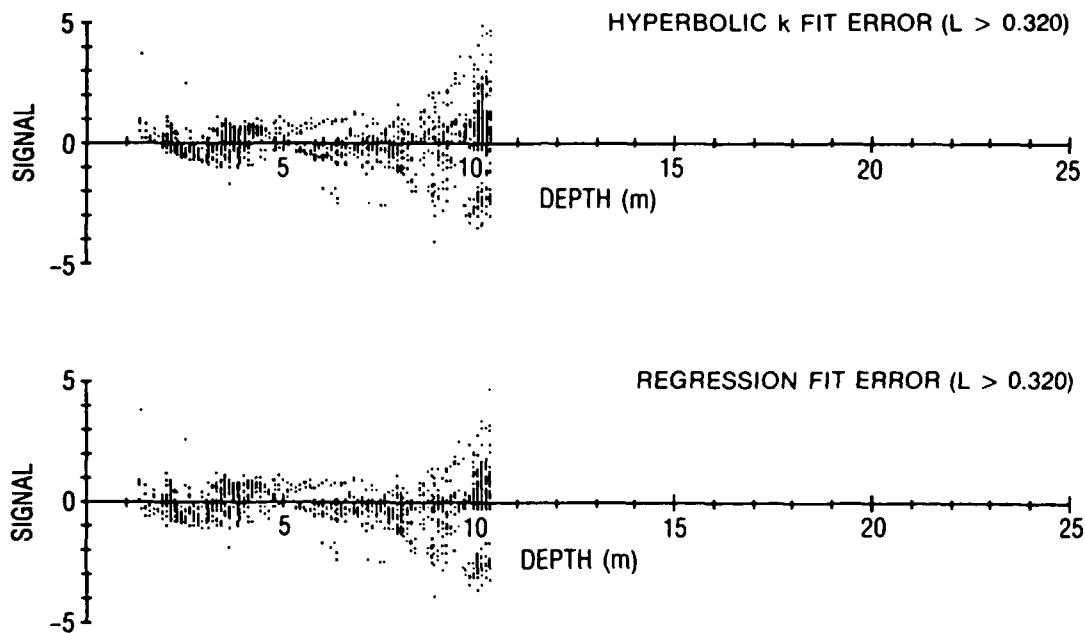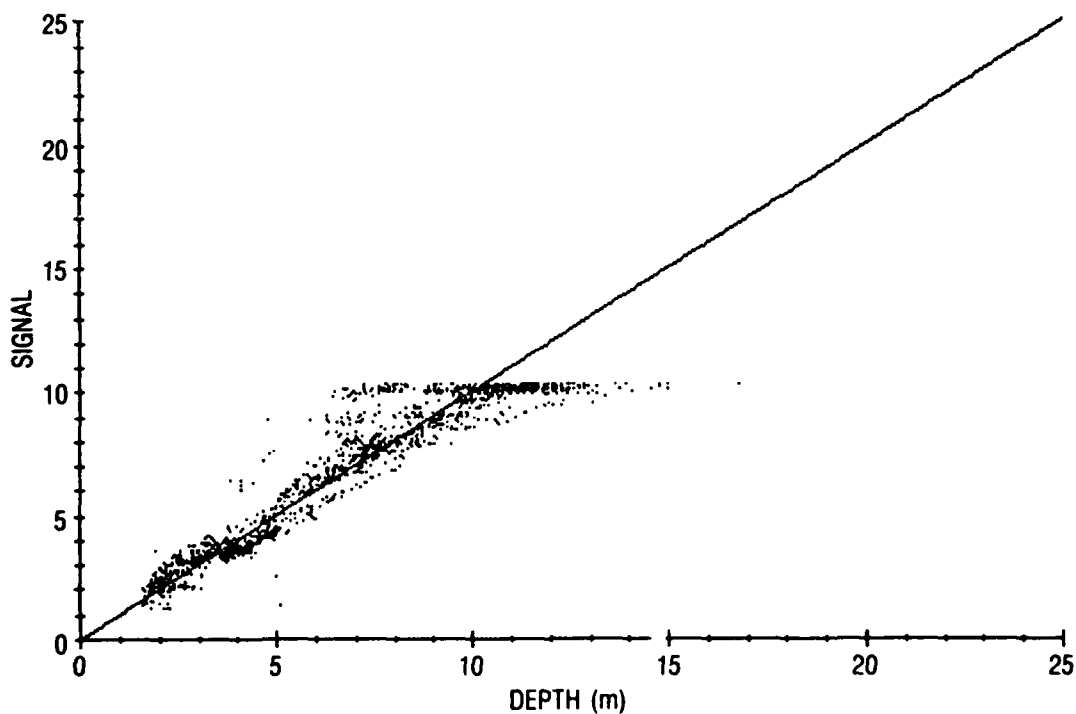
Figure 5. L1 vs depth.

Figure 6. Calculated - actual depth vs depth.

Figure 7. L1 : calculated depth vs actual depth.

Table 1. TUPS Sensor Configuration, June, 1988.

CHANNEL	SENSOR	S/N
1	Temperature sensor Sea Bird, Inc.	SBE3-638
2	Conductivity sensor Sea Bird, Inc.	SBE4-234
3	465 nm Upwelling Light Biospherical Instr.	MCP-200H-7129
4	507 nm Upwelling Light Biospherical Instr.	MCP-200H-7130
5	532 nm Upwelling Light Biospherical Instr.	MCP-200H-7131
6	Transmissometer Sea Tech, Inc.	165
7	Fluorometer, Sea Mar Tech, Inc. (signal)	6000AR-235
8	Fluorometer, Sea Mar Tech, Inc. (scale)	6000AR-235
9	488 nm Downwelling Light, Biospherical Instr.	QCP-200LM-7101
10	Echo Sounder Ulvertech, LTD.	205

Table 2. TESS Sensor Configuration, June, 1988.

CHANNEL	SENSOR
1	Voltage Reference, 2.5V, Analog Devices AD580M
2	Pyroheliometer 1, light bulb, Eppley Instr. Model 50, S/N 3039
3	Pyroheliometer 2, hemisphere, Eppley Instr. Model PSP, S/N 8022D1
4	488 nm Light (linear), Biospherical Instr. Model QCP-200HM-488, S/N 7105
5	441 nm Light (log), Biospherical Instr. Model QCP-200LM-441, S/N 7102

Table 3. Correlation Matrix of TUPS and TESS Measurements.

VARIABLE	TESSPYRO1	TESSPYRO2	465 nm	507 nm	532 nm	DEPTH
TESSPYRO1	1					
TESSPYRO2	0.997	1				
465 nm	0.379	0.380	1			
507 nm	0.367	0.366	0.989	1		
532 nm	0.336	0.336	0.975	0.995	1	
DEPTH	0.195	0.201	-0.235	-0.329	-0.374	1

Table 4. Single Band Regression

DEPTH	L1 RM	L1 RMS	L2 RM	L2 RMS	L3 RM	L3 RMS
0-5	0.906	0.4002	0.891	0.4105	0.890	0.3985
3-5	0.766	0.3134	0.707	0.3359	0.694	0.3383
0-10	0.956	0.7541	0.962	0.6963	0.964	0.6845
3-10	0.946	0.7679	0.957	0.6736	0.960	0.6477
0-15	0.914	1.488	0.976	0.7978	0.982	0.7045
3-15	0.891	1.530	0.972	0.7922	0.980	0.6780
0-17	0.907	1.657	0.976	0.8782	0.982	0.7637
3-17	0.884	1.705	0.972	0.8867	0.979	0.7445
0-22	0.873	3.214	0.933	2.357	0.929	2.432
3-22	0.853	3.288	0.925	2.377	0.920	2.440

Table 5. Two Band Regression

DEPTH	L1, L2		L1, L3		L2, L3	
	RM	RMS	RM	RMS	RM	RMS
0-5	0.911	0.3934	0.906	0.3971	0.893	0.4032
3-5	0.851	0.2912	0.796	0.3108	0.710	0.3359
0-10	0.962	0.6953	0.964	0.6795	0.964	0.6860
3-10	0.958	0.6689	0.960	0.6465	0.961	0.6368
0-15	0.980	0.7380	0.983	0.6941	0.983	0.6996
3-15	0.977	0.7208	0.981	0.6596	0.982	0.6511
0-17	0.979	0.8389	0.982	0.7529	0.983	0.7537
3-17	0.976	0.8356	0.980	0.7307	0.981	0.7190
0-22	0.935	2.339	0.934	2.327	0.934	2.325
3-22	0.926	2.355	0.925	2.372	0.927	2.348

Table 6. Three Band Regression

L1, L2, L3		
DEPTH	RM	RMS
0-5	0.940	0.3550
3-5	0.894	0.2654
0-10	0.964	0.6785
3-10	0.961	0.6368
0-15	0.983	0.6937
3-15	0.982	0.6562
0-17	0.983	0.7469
3-17	0.981	0.7212
0-22	0.936	2.297
3-22	0.928	2.322

Table 7. Hyperbolic k Fits

	L1: A = 0.489 B = 0.187	L2: A = 0.260 B = 0.145	L3: A = 0.180 B = 0.136
DEPTH	RMS	RMS	RMS
0-5	0.4754	0.6366	0.6392
3-5	0.4635	0.6652	0.6276
0-10	0.7511	0.6628	0.6319
3-10	0.7826	0.6802	0.6251
0-15	1.479	0.7816	0.6748
3-15	1.533	0.7984	0.6750
0-17	1.593	0.8559	0.7355
3-17	1.649	0.8803	0.7402
0-22	3.658	1.902	2.156
3-22	3.754	1.952	2.210